Cell Type-Specific Profiles and Developmental Trajectories of Transcriptomes in Primate Prefrontal Layer 3 Pyramidal Neurons: Implications for Schizophrenia

Dominique Arion, Ph.D., John F. Enwright III, Ph.D., Guillermo Gonzalez-Burgos, Ph.D., David A. Lewis, M.D.

Objective: In schizophrenia, impaired working memory is associated with transcriptome alterations in layer 3 pyramidal neurons (L3PNs) in the dorsolateral prefrontal cortex (DLPFC). Distinct subtypes of L3PNs that send axonal projections to the DLPFC in the opposite hemisphere (callosal projection [CP] neurons) or the parietal cortex in the same hemisphere (ipsilateral projection [IP] neurons) play critical roles in working memory. However, how the transcriptomes of these L3PN subtypes might shift during late postnatal development when working memory impairments emerge in individuals later diagnosed with schizophrenia is not known. The aim of this study was to characterize and compare the transcriptome profiles of CP and IP L3PNs across developmental transitions from prepuberty to adulthood in macaque monkeys.

Methods: The authors used retrograde labeling to identify CP and IP L3PNs in the DLPFC of prepubertal, postpubertal, and adult macaque monkeys, and used laser microdissection to capture these neurons for RNA sequencing.

Results: At all three ages, CP and IP L3PNs had distinct transcriptomes, with the number of genes differentially expressed between neuronal subtypes increasing with age. For IP L3PNs, age-related shifts in gene expression were most prominent between prepubertal and postpubertal animals, whereas for CP L3PNs such shifts were most prominent between postpubertal and adult animals.

Conclusions: These findings demonstrate the presence of cell type–specific profiles and developmental trajectories of the transcriptomes of PPC-projecting IP and DLPFC-projecting CP L3PNs in monkey DLPFC. The evidence that IP L3PNs reach a mature transcriptome earlier than CP L3PNs suggests that these two subtypes differentially contribute to the maturation of working memory performance across late postnatal development and that they may be differentially vulnerable to the disease process of schizophrenia at specific stages of postnatal development.

Am J Psychiatry 2024; 181:920-934; doi: 10.1176/appi.ajp.20230541

Certain core clinical features of schizophrenia, such as working memory impairments, appear to reflect, at least in part, alterations in the transcriptome of layer 3 pyramidal neurons (L3PNs) in the dorsolateral prefrontal cortex (DLFPC) (1). These neurons comprise different subtypes that are distinguished by the target of their principal axon projection. For example, the separate populations of L3PNs (2–4) that send axonal projections to either the posterior parietal cortex (PPC) in the ipsilateral hemisphere (ipsilateral projection [IP] L3PNs) or to the DLPFC in the contralateral hemisphere (callosal projection [CP] L3PNs) are both critical for working memory (5–8).

In monkey DLPFC, L3PNs undergo substantial anatomical changes across postnatal development that might contribute to the neural substrate for the maturation of working memory during adolescence and into early adulthood (9, 10). For example, although the principal axons of L3PNs in the primate neocortex reach their target areas before or shortly after birth (11, 12), the terminals of these axons change substantially during late postnatal development (10). Moreover, in monkey DLPFC, peak synaptic and dendritic spine densities on L3PNs are achieved 3–4 months after birth, followed by a plateau phase and then a protracted period, between $\sim\!2$ and $\sim\!5$ years of age, of pruning of excitatory synapses and dendritic spines (13, 14). Similar processes occur in human DLPFC, with pruning of dendritic spines on L3PNs continuing into the third decade of life (15).

We previously demonstrated that DLPFC-projecting CP L3PNs and PPC-projecting IP L3PNs in the monkey DLPFC exhibit numerous gene expression differences in postpubertal macaque monkeys (16). However, the developmental trajectories of L3PN transcriptomes across late

See related feature: Editorial by Dr. Arnsten and Dr. Datta (p. 861)

postnatal development from prepuberty to adulthood remain unknown. Knowledge of the timing and cell type specificity of these developmental trajectories is critical for understanding their contributions to the maturation of working memory (9) and for how alterations in these trajectories could contribute to the emergence and progression of working memory impairments during adolescence in individuals who are later diagnosed with schizophrenia (17–21).

Here we sought to characterize and compare the transcriptome profiles of CP and IP L3PNs across developmental transitions from prepuberty to adulthood in macaque monkeys. We used laser microdissection to individually dissect retrogradely labeled homotopic DLPFC-projecting CP L3PNs and PPC-projecting IP L3PNs from the DLPFC of prepubertal, postpubertal, and adult animals and subjected pools of these neurons from each monkey to RNAseq analyses. We found that expression levels of the genes that distinguish these two L3PN subtypes change substantially across the peripubertal period and into adulthood, with the transcriptome of IP L3PNs reaching a mature state earlier than CP L3PNs. These transcriptome differences between, and distinct developmental trajectories of, two key neuronal subtypes that subserve working memory suggest that each L3PN subtype 1) might differentially contribute to the normal maturation of working memory function and 2) might be differentially vulnerable to risk factors for schizophrenia occurring at specific postnatal ages.

METHODS

Animals, Surgical Procedures, and Laser Microdissection Methods

Nine prepubertal (mean age, 19.7 months [SD=1.7]; five females and four males), eight postpubertal (mean age, 38.5 months [SD=0.9]; four females and four males), and eight adult (mean age, 56.6 months [SD=1.8]; four females and four males) Rhesus macaque monkeys (*Macaca mulatta*) were used in these studies (see Table S1 in the online supplement). For the postpubertal animals, we obtained new data from a subset of these animals (see Table S1, RNAseq Batch 2) and we reanalyzed our published data (16) from five of these animals (see Table S1, RNAseq Batch 1).

All housing and experimental procedures were conducted in accordance with U.S. Department of Agriculture and National Institutes of Health guidelines and were approved by the University of Pittsburgh Institutional Animal Care and Use Committee. All monkeys were subjected to identical surgical procedures (see the online supplement). Injections of inert red (Alexa Fluor 555, Invitrogen-ThermoFisher) or green (Alexa Fluor 488, Invitrogen-ThermoFisher) fluorescent-labeled cholera toxin subunit B were made in the right DLPFC and in the left PPC (see Figure S1 in the online supplement), as previously described (16). Two weeks after surgery, animals were euthanized using methods consistent with the American Veterinary Medical Association Guidelines for the Euthanasia of Animals. Brains were immediately removed and cut into coronal blocks, which were flash-frozen and stored at -80° C.

From the left DLPFC of each monkey, cryostat sections (16 $\,\mu m)$ were mounted onto polyethylene naphthalate membrane slides (Leica Microsystems, Buffalo Grove, IL) and fluorescently labeled neurons (i.e., CP neurons labeled from the injections in the right DLPFC and IP neurons labeled from the injections in the left PPC) in layer 3 were individually dissected from DLPFC area 46 (see the Supplementary Methods section and Figure S1 in the online supplement). For each cell type, 120 neurons were pooled into one sample, and two such samples were collected from each monkey. For some monkeys, only one region was injected, and thus samples were obtained for only one cell type (see Table S1 in the online supplement).

Library Preparation, Sequencing, and Bioinformatic Analysis

Total RNA was extracted from each pooled sample of neurons using the QIAGEN RNeasy Plus Micro kit (QIA-GEN, Germantown, MD). Libraries were generated with the Takara SMART-Seq Stranded kit using Takara SMARTer RNA Unique Dual Index A and B Kits (Takara, Mountain View, CA). Sequencing was performed using the NovaSeq 6000 platform (Illumina, San Diego) to an average of 50 million 101-bp paired-end reads. Several quality control measures, including Phred scores and sequencing statistics, confirmed the presence of high-quality samples (see the Supplementary Methods section, Table S2, and Figure S2 in the online supplement). Moreover, pilot samples, identical to those used in this study, generated clearly visible 28S and 18S profiles on an Agilent Screen Tape system, and cDNA synthesis for these samples generated libraries with a size (356 bp, SD=8.1) and concentration (27 ng/ μ L, SD=10.1) that are consistent with high RNA quality.

Counts for the replicate samples (which were highly correlated; all r values >0.98) were then combined to increase sequencing depth, resulting in 36 final samples for differential expression analysis. Filtering processes (see the Supplementary Methods section in the online supplement) resulted in the detection of 12,250 unique genes that were used for differential gene expression analysis between L3PN subtypes within an age group or within an L3PN subtype across age groups. The log₂ counts per million (CPM) values, along with the precision weights obtained during voom normalization, were used with the *limma* package, version 3.56.2 (22). This same pipeline was used to reanalyze data from our previously published study of postpubertal monkeys (16).

Comparison of Gene Expression Between Cell Types Within Age Groups and Within Cell Types Across Age Groups

For analyses comparing CP to IP neurons within each age group, the Combat function of the Surrogate Variable Analysis package (version 3.48.0) in R (23) was used on the filtered log₂ CPM values to mitigate the robust effect of monkey, and sex was included as a covariate during the statistical modeling in *limma*. Because it was not possible to

collect both cell types from all animals, to maintain a strict within-animal paired design for the within-age-group analysis, only a subset of the new prepubertal and adult samples were used (i.e., those from which both CP and IP L3PNs were collected from each animal; see Table S1 in the online supplement). This approach resulted in the analysis of data from both CP and IP L3PNs from five prepubertal, five postpubertal, and seven adult monkeys. Within each age group, differentially expressed genes (DEGs) between CP and IP L3PNs were determined using the Benjamini-Hochberg procedure with a false discovery rate (FDR) of 5% (see the Supplementary Methods section in the online supplement).

For comparisons within each L3PN subtype across age groups, separate analyses for CP and IP L3PNs were conducted using new samples (see Table S1, RNAseq Batch 2, in the online supplement) from prepubertal (eight CP and six IP samples), postpubertal (five CP and two IP samples), and adult animals (eight CP and seven IP samples). After validating that the RNAseq Batch 2 data were consistent with the findings from RNAseq Batch 1 (see the Supplementary Results section in the online supplement), we performed analyses on the Batch 2 data using the filtered log₂ CPM values without correction for monkey. For each cell type, an analysis of variance (ANOVA) in limma using sex as a covariate with a 5% FDR across the three age groups was used to identify genes differentially expressed with age. Only genes significant in the ANOVA were retained for subsequent analyses between consecutive age groups (see the Supplementary Methods section in the online supplement). Additionally, because of the small difference in expression levels for many DEGs, subsequent analyses of within-age-group and between-cell-type comparisons were focused primarily on DEGs with a log₂ fold difference $(DEG_{FD}) \ge 0.2$ (i.e., $\ge 15\%$). However, the entire set of genes was used for pathway analysis. Specifically, gene set enrichment analysis using fast Gene Set Enrichment Analysis (fGSEA, version 1.26.0), a threshold-free approach, was performed in R (24) using the human gene ontology (GO) pathways for Biological Process, Cellular Component, and Molecular Function. Only pathways with q<0.05 are reported as significant. All genes were ranked using the test statistic derived from the differential expression analysis, and the fGSEA option to collapse highly overlapping pathways was implemented.

To perform threshold-free analyses on the overall patterns of gene expression shifts during development, and to compare the present findings to our previously published data (16), rank-rank hypergeometric overlap (RRHO) analyses were performed using the R package RRHO2 (25). The "hyper" method with a step size of 10 was used for all analyses to determine concordant/discordant gene expression patterns and to generate RRHO2 plots.

RESULTS

Confirmation of Microdissected Neurons as L3PNs

To verify that the pools of individually microdissected, retrogradely labeled neurons comprised L3PNs, we assessed

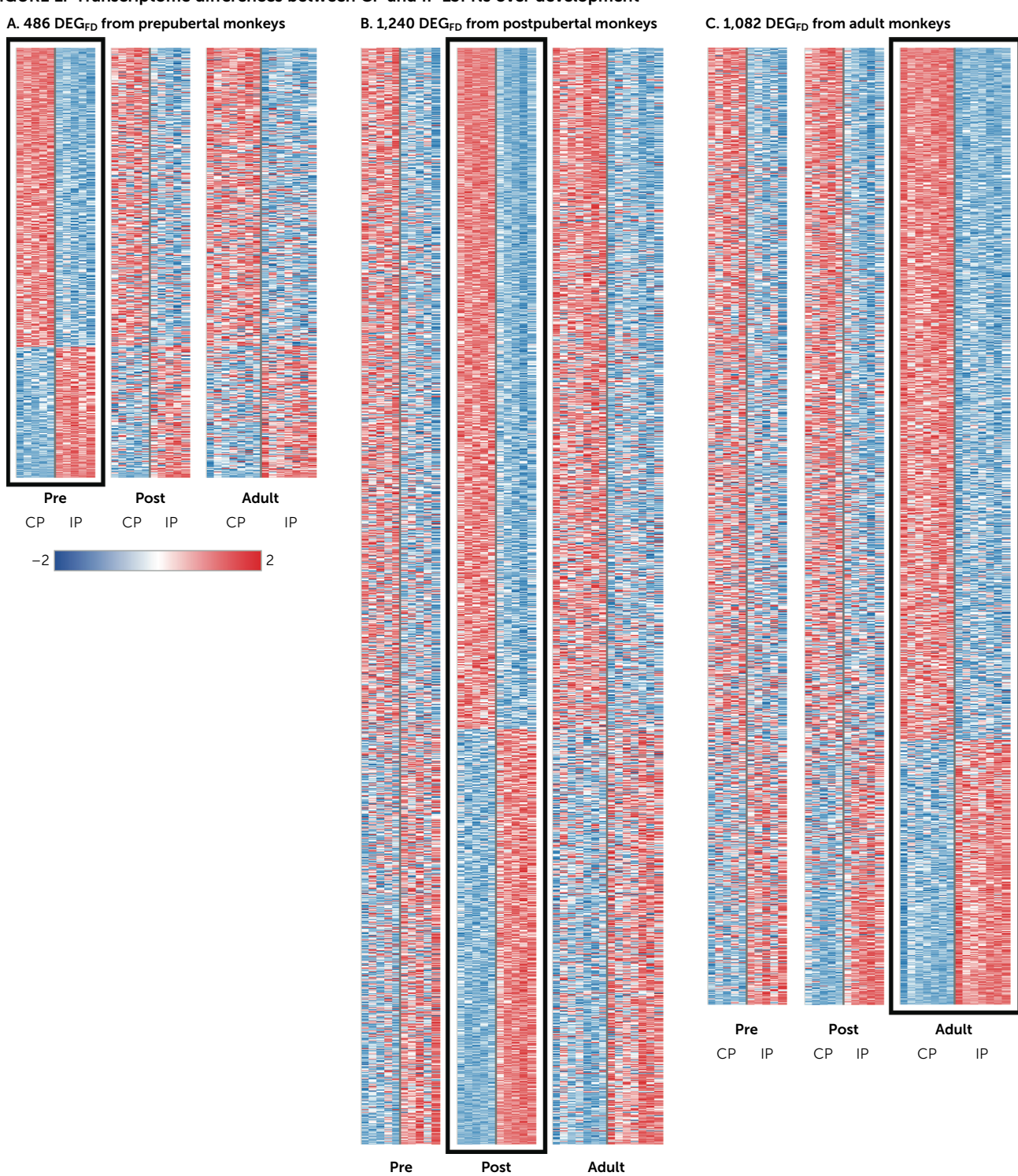
the ratios of two sets of genes. We first compared the levels of a marker of DLPFC layers 2–3, Cut-like homeobox 2 (CUX2), to a marker of DLPFC layers 5–6, Fez family zinc finger protein (FEZF2) (26). In each sample, the CUX2/FEZF2 ratio was \geq 48. We also compared the levels of the excitatory neuron marker SLC17A7 (vesicular glutamate cotransporter 1) to the inhibitory neuron marker SLC32A1 (vesicular GABA transporter). In each sample, the SLC1747/SLC32A1 ratio was \geq 54. Together, these findings confirm that all samples contain primarily L3PNs.

Comparison of Gene Expression Levels Between CP and IP L3PNs Within Each Age Group

Our previous study of postpubertal monkeys (16) detected numerous genes with significantly different expression levels between CP and PPC-projecting IP L3PNs in the DLPFC. To determine whether the transcriptomes of CP and IP L3PNs differ with age, we analyzed gene expression in DLPFC CP and IP L3PNs from prepubertal and adult monkeys (see Table S1 in the online supplement) and we reanalyzed data from the prior study of postpubertal monkeys (16) using the new analytical pipeline applied to the prepubertal and adult animals. These within-age-group analyses showed that the number of DEGs between CP and IP L3PNs increased from 1,046 DEGs in prepubertal animals to 1,942 DEGs in postpubertal animals and to 3,057 DEGs in adult animals. Because the magnitude of these statistically significant differences was modest for some transcripts, we focused subsequent analyses on those DEGs that had a \log_2 fold difference (DEG_{FD}) of ≥ 0.2 (i.e., $\geq 15\%$). This focus reduced the number of genes differentially expressed between CP and IP L3PNs to 486 DEG_{FD} in prepubertal animals (Figure 1A), 1,240 DEGFD in postpubertal animals (Figure 1B), and 1,082 DEG_{FD} in adult animals (Figure 1C). To further assess the robustness of these findings, we used a second statistical approach that did not correct for monkey (see the Supplementary Methods section in the online supplement). This approach confirmed that the number of DEGs increased with age (see Figure S3A in the online supplement). In addition, the findings from the two approaches were highly correlated (see Figure S3B in the online supplement). Together, these analyses demonstrate that the number of gene expression differences between CP and IP L3PNs is greater in adult than prepubertal monkeys. Moreover, sex was not detected as a significant determinant of the transcriptome in either cell type in any age group in any analysis.

Pathway analysis using fGSEA detected 67, 123, and 138 pathways in prepubertal, postpubertal, and adult animals, respectively, that were enriched in CP or IP L3PNs relative to the other cell type (see Table 1 for the top 10 pathways enriched in each cell type at each age and the online supplement for lists of all significant pathways). Most of these pathways were enriched in IP L3PNs in prepubertal (84%) and postpubertal (76%) animals, whereas 58% of the pathways were enriched in CP L3PNs in adult animals.

FIGURE 1. Transcriptome differences between CP and IP L3PNs over development^a



^a In each heatmap, rows indicate individual genes and columns represent individual monkeys within each age group. In panel A, the bold outline indicates a heat map of genes qualifying as DEG_{FD} between CP and IP L3PNs in prepubertal animals. The adjacent heat maps show the relative expression levels of these same genes in postpubertal and adult animals. In panel B, the bold outline indicates a heat map of genes qualifying as DEG_{FD} between CP and IP L3PNs in postpubertal animals. The adjacent heat maps show the relative expression levels of those same genes in prepubertal and adult animals. In panel C, the bold outline indicates a heat map of genes qualifying as DEG_{FD} between CP and IP PNs in adult animals. The adjacent heat maps show the relative expression levels of those same genes in prepubertal and postpubertal animals. In all three panels, the DEG_{FD} in the highlighted age group show a similar pattern of differential gene expression in the other two age groups. CP=callosal projection; DEG_{FD} =differentially expressed genes with log_2 fold difference ≥ 0.2 ; IP=ipsilateral projection; L3PNs=layer 3 pyramidal neurons; PR=prepubertal; PR=postpubertal.

CP

ΙP

CP IP

CP IP

TABLE 1. Top 10 pathways differentiating CP from IP neurons in each age group^a

TABLE 1. Top 10 pathways differentiation	ng CP Irom I						
CP-Enriched Pathways	p _{adj}	NES	Size	IP-Enriched Pathways	p _{adj}	NES	Size
Prepubertal				Prepubertal			
GOBP positive regulation of protein targeting to membrane	4.02E-03	2.04	24	GOMF structural constituent of cytoskeleton	8.12E-05	2.30	66
GOBP forelimb morphogenesis	1.33E-02	2.01	16	GOCC intermediate filament	8.22E-04	2.23	42
GOBP anterior/posterior axis	2.62E-02	1.92	22	GOCC myelin sheath	2.80E-03	2.14	19
specification	2.02L 02	1.52	22	GOBP positive regulation of	4.49E-03		35
GOBP gamma-aminobutyric acid	2.90E-02	1.92	22	potassium ion transmembrane	1.132 00	2.10	33
signaling pathway	2.502 02	1.52		transporter activity			
GOCC cytosolic ribosome	1.90E-03	1.91	89	GOBP intermediate filament-based	4.02E-03	2.10	32
GOBP positive regulation of epithelial	2.93E-02	1.88	24	process			
cell differentiation				GOBP protein localization to	4.95E-03	2.08	28
GOBP cellular response to	1.32E-02	1.81	71	lysosome			
calcium ion				GOMF ATP-dependent protein	7.41E-03	2.06	17
GOBP cytoplasmic translation	2.61E-03	1.79	143	folding chaperone			
GOBP regulation of epithelial to	1.77E-02	1.78	63	GOBP vesicle docking involved in	5.38E-03	2.05	42
mesenchymal transition				exocytosis			
GOBP negative regulation of cell-cell	1.03E-02	1.78	88	GOBP regulation of vesicle fusion	1.13E-02	2.04	47
adhesion				GOBP post-Golgi vesicle-mediated	1.01E-03	2.01	22
Postpubertal				transport			
GOBP positive regulation of epithelial	3.29E-03	2.03	24	Postpubertal			
cell differentiation				GOCC main axon	3.64E-09	2.67	55
GOBP regulation of epithelial cell	7.18E-04	1.95	68	GOCC inner mitochondrial	5.00E-09	2.49	110
differentiation				membrane protein complex			
GOBP negative regulation of cell	5.01E-04	1.91	89	GOCC myelin sheath	1.24E-04	2.30	35
activation				GOBP aerobic respiration	3.21E-08	2.29	138
GOBP regulation of CD4-positive	2.65E-02	1.90	19	GOCC mitochondrial protein-	4.88E-10	2.19	242
alpha-beta T cell differentiation	c- oo			containing complex			
GOBP mRNA splice site selection	3.46E-02	1.81	31	GOBP proton transmembrane	4.00E-05	2.14	90
GOBP regulation of synapse assembly	7.78E-03	1.79	84	transport	2405 05	2.47	400
GOMF SMAD binding	1.40E-02 3.65E-03	1.78 1.77	61 105	GOMF primary active transmembrane	2.19E-05	2.13	108
GOCC postsynaptic specialization membrane	3.03E-03	1.//	105	transporter activity GOMF electron transfer activity	1.24E-04	2.10	77
GOBP alternative mRNA splicing via	1.60E-02	1.74	74	GOCC intermediate filament	1.33E-03	2.10	42
spliceosome	1.000-02	1./4	74	GOCC intermediate marrierit GOCC oxidoreductase complex	1.91E-04	2.10	86
GOBP lens development in camera-	2.36E-02	1.73	54	·	1.91L 04	2.03	00
type eye	2.50L 02	1.75	5-	Adult	4 445 47	2.00	440
				GOCC inner mitochondrial	1.41E-13	2.89	110
Adult	2.11E-06	2.00	0.4	membrane protein complex	1.005 13	2.07	90
GOBP long development in camera		2.09	84	GOBP proton transmembrane	1.80E-12	2.83	90
GOBP lens development in camera- type eye	1.07E-04	2.04	54	transport GOBP ATP metabolic process	1.80E-12	2.58	157
GOMF beta-catenin binding	2.71E-05	2.02	72	GOMF primary active transmembrane	5.52E-09	2.54	108
GOMF SMAD binding	1.03E-04	1.99	61		J.JZE-09	2.54	100
GOBP cell fate determination	3.41E-03	1.94	20	transporter activity GOMF ATPase-coupled cation	5.54E-05	2 70	38
GOBP labyrinthine layer blood vessel	1.85E-02	1.88	16	transmembrane transporter activity	J.J4L 0J	2.33	50
development	1.03L 02	1.00	10	GOCC mitochondrial protein-	5.65E-14	2.37	242
GOBP regulation of dendrite	2.75E-03	1.85	59	containing complex	3.03L 14	2.57	272
morphogenesis	2.73L 03	1.05	33	GOBP aerobic respiration	1.63E-08	2.35	138
GOBP cellular response to calcium ion	2.64E-03	1.83	71	GOCC oxidoreductase complex	5.41E-06	2.33	86
GOBP response to acetylcholine	1.83E-02	1.81	22	GOCC proteasome regulatory particle	1.36E-03	2.23	19
GOCC transcription repressor	2.71E-03		58	GOBP retrograde axonal transport	1.24E-03		18
·				and the second s			
complex							

^a CP=callosal projection; IP=ipsilateral projection; NES=normalized enrichment score.

Moreover, higher-order molecular processes specific to each cell type were conserved; for example, across age groups, pathways related to synaptic structure and translation/RNA processing were CP-enriched, and mitochondrial energy production and actin/cytoskeleton-related pathways were IP-enriched. Moreover, many of these pathways contained genes involved in basic neuronal functions such as action potential generation, synaptic vesicle release, or

cAMP-mediated signaling, and some of these genes were differentially expressed between L3PN subtypes in more than one age group. For example, in all three age groups, the voltage-gated sodium channel subunit gene SCN1A was enriched in IP neurons, whereas SCN3A was enriched in CP neurons (Figure 2). Similarly, among the synaptotagmin genes involved in vesicle release, SYT2 was enriched in IP neurons, whereas SYT10 was enriched in CP neurons from

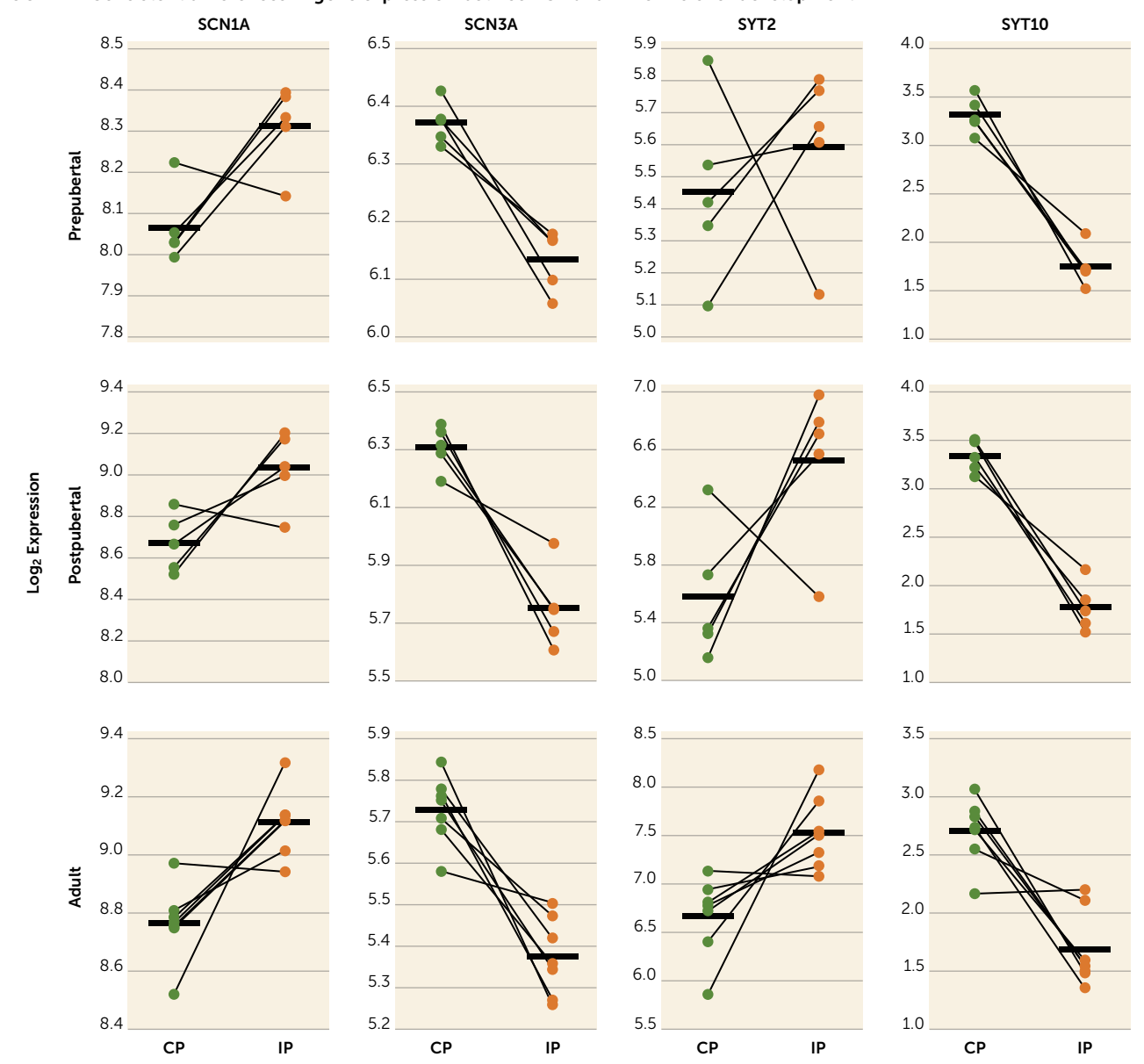


FIGURE 2. Consistent differences in gene expression between CP and IP L3PNs over development^a

all three age groups (Figure 2). Furthermore, in all three age groups, the structural gene NEFM was enriched in IP L3PNs (Figure 3), whereas genes whose products increase neurite outgrowth, such as HGF (27) (Figure 3), CELSR1 (28), ADCYAP1 (29), and TIAM1 (30), were enriched in CP L3PNs at all three ages.

Many genes identified as a DEG in only one age group nonetheless had a similar pattern of differential expression in every age group (see Figure S4 in the online supplement). These similarities are further illustrated in Figure 1. Specifically, for the $\rm DEG_{FD}$ in a given age group, a similar overall pattern of gene expression differences between cell types was evident in the other two age groups. Together, these

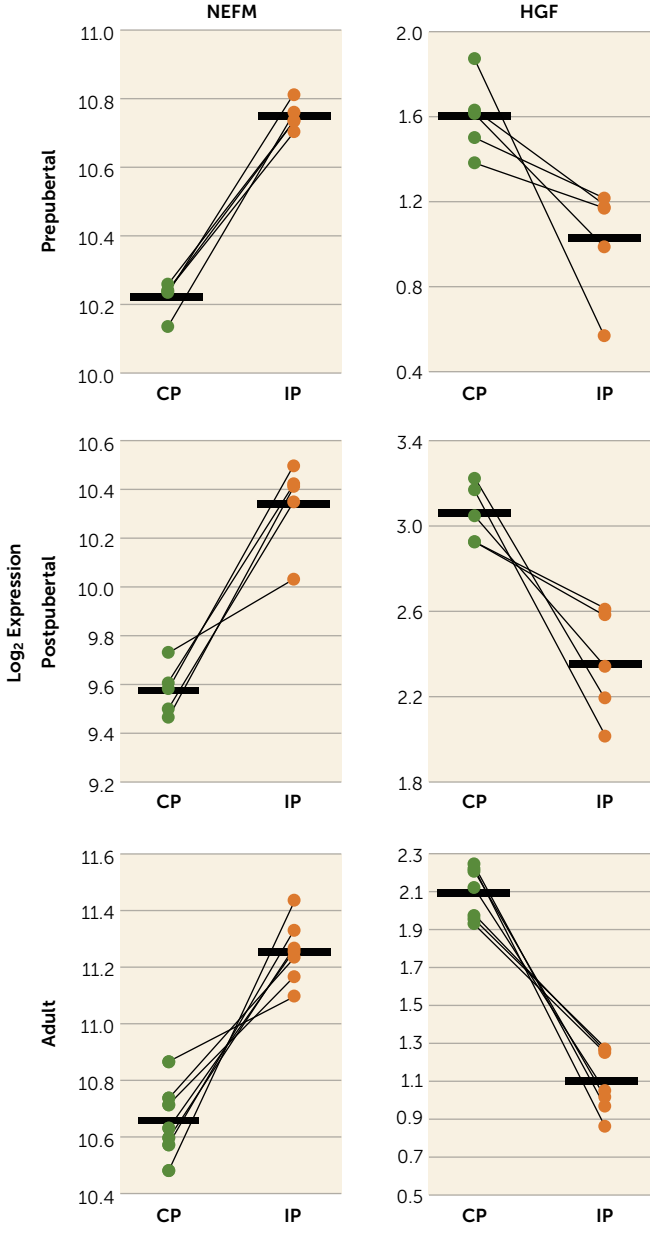
findings indicate that IP and CP L3PNs have distinct transcriptomes in prepubertal, postpubertal, and adult monkeys and that these gene expression differences become more prominent during late postnatal development.

Comparison of Gene Expression Levels in CP or IP L3PNs Across Age Groups

The above analyses revealed substantial differences in gene expression between CP and IP L3PNs within each age group. However, these analyses do not reveal whether the differences in numbers of DEG and $\rm DEG_{FD}$ between L3PN subtypes across age groups reflect developmental shifts in gene expression in CP L3PNs, in IP L3PNs, or in both L3PN

^a Plots of log₂ expression values for two voltage-gated sodium channels (SCN1A and SCN3A) and two synaptotagmins (SYT2 and SYT10) in CP and IP L3PNs from each age group. Hash bars indicate group means, and filled circles indicate values for individual monkeys; lines connect the CP and IP samples from each monkey. Log₂ expression values can be compared between L3PN subtypes within a given age group, but not across age groups due to the different sequencing batches. L3PNs=layer 3 pyramidal neurons; CP=callosal projection; IP=ipsilateral projection.

FIGURE 3. Examples of genes enriched in IP or CPL3PNs at all three developmental time points $^{\rm a}$



^a Plots of log₂ expression values for the structural gene NEFM and the neurite outgrowth gene HGF in CP and IP L3PNs from each age group. Hash bars indicate group means, and filled circles indicate values for individual monkeys; lines connect the CP and IP samples from each monkey. Log₂ expression values can be compared between L3PN subtypes within a given age group, but not across age groups due to the different sequencing batches. CP=callosal projection; IP=ipsilateral projection; L3PNs=layer 3 pyramidal neurons.

subtypes, because these within-age-group analyses used different RNA sequencing batches between the post-pubertal animals and the prepubertal and adult animals (see Table S1 in the online supplement). To address this limitation, we next examined the transcriptomes of CP and IP L3PNs from each age group that were processed in the same sequencing batch (see Table S1, RNAseq Batch 2, in the online supplement).

In CP neurons, ANOVA on Batch 2 data identified 736 DEGs across the three age groups (Figure 4A). The levels of most of these genes in the postpubertal animals were intermediate to those in the younger and older age groups (Figure 4A). For example, expression levels of SNTG2 and GABRG2 in CP neurons progressively increased with age (Figure 4B, top), whereas GABRA2 and SEMA5B expression levels progressively decreased with age (Figure 4B, bottom). Pathway analysis (see Table 2 for the top 10 pathways and the online supplement for all significant pathways) identified 37 pathways that differed between prepubertal and postpubertal animals; mitochondrial energy production, synaptic structure, and translation were enriched in prepubertal animals, and transcriptional regulation was enriched in postpubertal animals. In addition, 79 pathways differed between postpubertal and adult animals; synaptic structure and ion transport pathways were enriched in postpubertal animals, and translation, mitochondrial energy production, and synaptic-vesicle-related pathways were enriched in adult animals.

In IP neurons, ANOVA detected 660 DEGs across the three age groups, with the expression levels of many of these genes in the postpubertal animals intermediate to those from prepubertal and adult animals (Figure 4C). For example, WNT5A gene expression levels in IP L3PNs progressively increased with age, whereas SSTR1 levels progressively decreased with age (Figure 4D). Pathway analysis (see Table 3 for the top 10 pathways and the online supplement for all significant pathways) detected 37 pathways that differed between prepubertal and postpubertal monkeys. Pathways enriched in prepubertal IP L3PNs contained many overlapping gene sets involved in synapse structure, whereas those enriched in the postpubertal animals were involved in mitochondrial energy production. Thirteen pathways differed between postpubertal and adult IP L3PNs (Table 3); pathways enriched in adult animals were related to translation, whereas the pathways enriched in the postpubertal animals were primarily involved in calcium transport.

Comparison of these analyses within each cell type suggests that CP and IP L3PNs differ in the developmental timing of their largest shifts (i.e., $\geq 15\%$) in gene expression. For example, in the transition between prepuberty and postpuberty, 49.5% (364) of the 736 DEGs in CP L3PNs were identified as DEG_{FD}, compared to 73.5% (485) of the 660 DEGs in IP neurons (χ^2 =83.3, df=1, p<0.00001). In contrast, in the transition between postpuberty and adulthood, 59.8% (440) of the 736 DEGs in CP L3PNs, but only 39.4% (260) of the 660 DEGs in IP L3PNs qualified as DEG_{FD} $(\chi^2=57.9, df=1, p<0.00001)$. These differences between CP and IP L3PNs in the timing of their developmental shifts in gene expression are illustrated by specific genes. For example, SEPTIN4 levels in CP L3PNs increased by 20% between prepuberty and postpuberty but by 61% between postpuberty and adulthood, whereas in IP L3PNs, SEPTIN4 levels increased by 70% between prepuberty and postpuberty but did not differ between postpuberty and adulthood

(Figure 4E, left). Similarly, for NEFM levels, the larger developmental increase in CP L3PNs was between postpuberty and adulthood, whereas in IP L3PNs the larger increase was between prepuberty and postpuberty (Figure 4E, right). Together, these findings suggest that IP L3PNs approach a mature transcriptome state earlier during postnatal development than do CP L3PNs.

RRHO2 Analyses Corroborate Differential Timing of Shifts in Gene Expression Between Cell Types

Although many of the differences between CP and IP L3PNs are present in prepubertal animals, the threshold-based analyses above suggest that these two cell types differ in the timing of the maturation of their transcriptomes. To explore this idea more fully, we evaluated all the genes in our data set using RRHO2, a threshold-free approach that does not depend on statistical cutoffs. Many genes that differed in expression level over development showed concordant changes in CP and IP L3PNs. For example, between the prepubertal and postpubertal animals, 4,279 genes concordantly increased in expression and another 3,038 genes concordantly decreased in expression in both CP and IP L3PNs (Figure 5A). However, for 796 genes the differences in gene expression patterns between these age groups were discordant between CP and IP L3PNs, suggesting that the expression of these genes was changing in only one cell type or changing in opposite directions in each cell type. Analysis of the expression levels of these individual genes (Figure 5C) showed a much larger change in expression in IP compared to CP L3PNs between the prepubertal and postpubertal age groups, with most of these genes increasing in expression over this developmental transition.

Shifts in gene expression were also present between the postpubertal and adult age groups, with 3,825 genes concordantly increasing in expression with age in both cell types and 2,563 genes concordantly decreasing with age (Figure 5B). An additional 1,455 genes had discordant gene expression between CP and IP L3PNs over this transition. Analysis of the expression levels of these individual genes (Figure 5D) showed a much larger change in expression in CP compared to IP L3PNs between the postpubertal and adult age groups, with most of these genes decreasing in expression over this developmental transition.

The discordant gene expression analyses above support the idea that the maturation of IP L3PNs precedes that of CP L3PNs. To test this hypothesis, we examined the gene expression patterns for all genes over these developmental epochs. Specifically, for each cell type we used an RRHO2 analysis to compare the gene expression differences between the prepubertal and adult animals to the differences in expression of these genes during the prepubertal-to-postpubertal transition and during the postpubertal-to-adult transition. As shown in Figure 5E, the earlier transition accounts for most of the overall difference with age for IP L3PNs, whereas the later transition accounts for more of the overall difference with age for CP L3PNs, findings consistent with an

earlier transcriptional maturation of IP L3PNs and a later transcriptional maturation of CP L3PNs.

Together, the findings using threshold-based cutoffs and the findings using threshold-free approaches of both discordant and overall gene expression patterns converge on the interpretation that developmental shifts in gene expression characteristic of the adult state occur earlier in IP L3PNs than in CP L3PNs.

DISCUSSION

We identified numerous shifts during late postnatal development in the gene expression profiles of both DLPFCprojecting CP L3PNs and PPC-projecting IP L3PNs from macaque monkeys. Our findings demonstrate that 1) the transcriptomes of CP and IP L3PNs substantially differ at each of the three ages studied; 2) the number of genes and gene pathways differentiating CP from IP L3PNs increases with age; 3) these age-related differences between cell types appear to be the consequence of developmental shifts in gene expression in both cell types; and 4) the larger shift in gene expression took place between prepubertal and postpubertal animals for IP L3PNs but between postpubertal and adult animals for CP L3PNs. These findings indicate that the developmental trajectories of DLPFC CP and IP L3PN transcriptomes are protracted and differ in timing based on cell type.

Transcriptome Differences Between CP and IP L3PNs

In the DLPFC of adult macaque monkeys, CP and IP L3PNs are distinct anatomical populations (2-4). We previously identified numerous genes that were differentially expressed between these populations in postpubertal monkeys (16). Here, we show that many genes are also differentially expressed between CP and IP L3PNs earlier in development in the prepubertal period, consistent with prior findings that patterns of gene expression can be used to distinguish pyramidal neuron (PN) subtypes in prepubertal mice (31) and humans (32). We also found that a core set of large transcript differences between these PN subtypes persists into adulthood. Specifically, 132 genes met criteria for DEG_{FD} in all three age groups. In concert, these molecular findings support the anatomical data that DLPFC-projecting CP L3PNs and PPC-projecting IP L3PNs in monkey DLPFC are distinct populations of neurons, and they provide a molecular signature of each cell type that might make them identifiable in clustering algorithms applied to single nucleus RNAseq data.

Consistent with this idea of distinct molecular-anatomical phenotypes of subtypes of L3PNs, some of the identified DEGs might contribute to other morphological differences between CP and IP L3PNs, such as the larger somal size, greater dendritic length and complexity, and higher spine density of CP relative to IP L3PNs in monkey DLPFC (11, 33). For example, the heavy neurofilament gene, NEFM, an axonal cytoskeleton protein (34), showed higher expression in IP

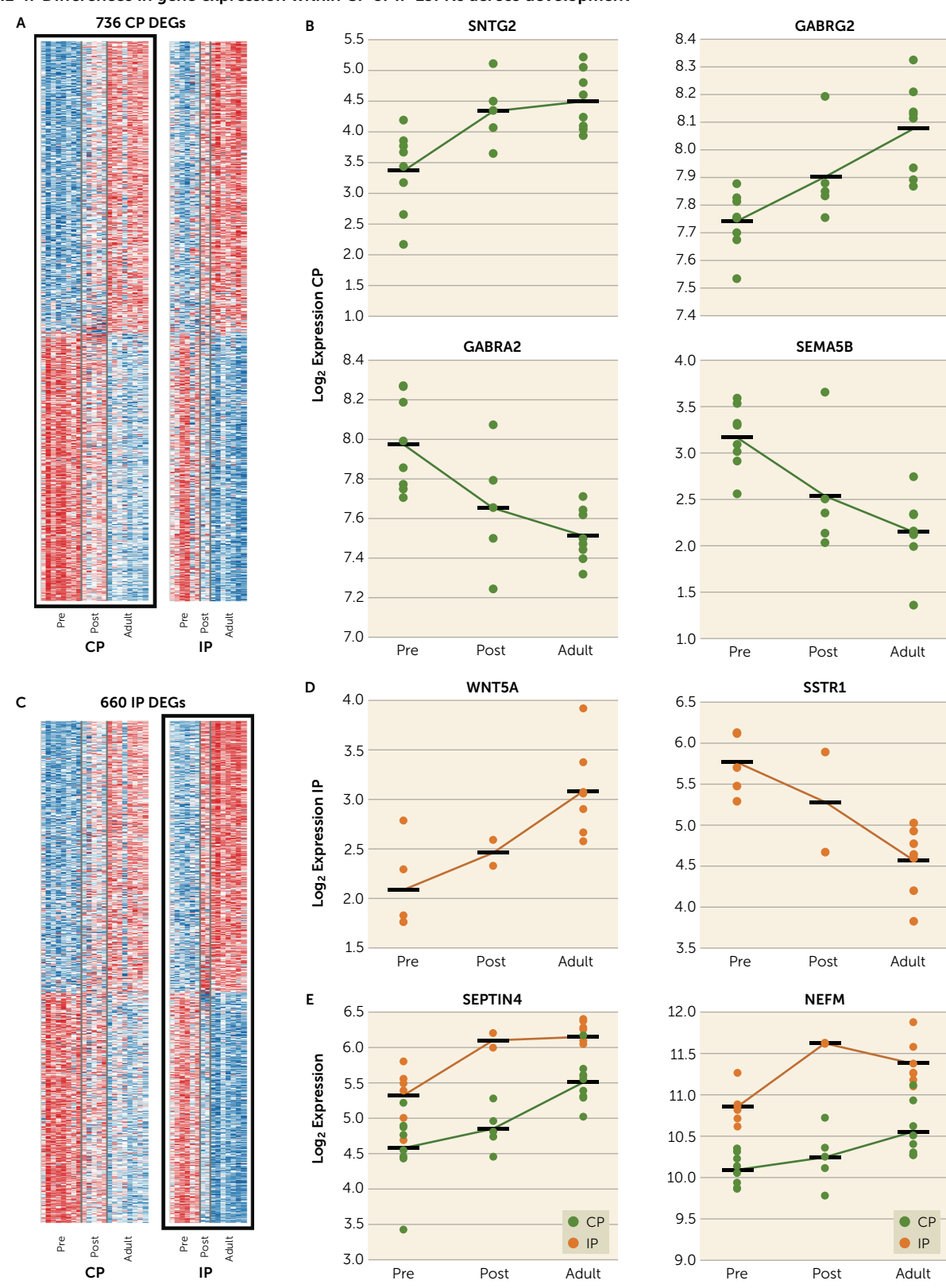


FIGURE 4. Differences in gene expression within CP or IP L3PNs across development^a

^a In panel A, the bold outline indicates a heat map of genes whose expression levels in CP L3PNs differ across the three age groups studied. The heat map to the right shows the expression levels of those same genes in IP L3PNs. Panel B shows plots of DEGs in CP L3PNs with progressively increasing (top) or declining (bottom) expression levels over late postnatal development. In panel C, the bold outline indicates a heat map of genes whose expression levels in IP L3PNs differ across the three age groups studied. The heat map to the left shows the expression levels of those same genes in CP L3PNs. Panel D shows plots of DEGs in IP L3PNs with progressively increasing (left) or declining (right) expression levels over late postnatal development. Panel

TABLE 2. Top 10 significant pathways in CP L3PNs differentiating prepubertal and adult animals from postpubertal animals

Pathways	p _{adj}	NES	Size	Pathways	p _{adj}	NES	Size
Prepubertal-enriched versus postpubertal				Postpubertal-enriched versus adult			
GOCC proteasome core complex	9.87E-05	2.42	16	GOCC intrinsic component of	6.70E-04	2.17	52
GOBP postsynapse assembly	1.27E-02	2.11	27	postsynaptic density membrane			
GOMF G protein activity	1.57E-02	2.05	34	GOBP regulation of synapse assembly	1.53E-04	2.13	84
GOMF Wnt-protein binding	3.25E-02	2.03	18	GOBP regulation of synapse structure or	1.46E-06	2.10	175
GOBP heterophilic cell-cell adhesion	3.78E-02	1.97	28	activity			
via plasma membrane cell-adhesion molecules				GOBP adenylate cyclase-activating G protein-coupled receptor signaling	8.64E-04	2.04	67
GOBP granulocyte migration	3.60E-02	1.89	48	pathway			
GOCC intrinsic component of synaptic	4.91E-03	1.82	143	GOBP vocalization behavior	1.45E-02	2.03	16
membrane				GOBP synapse maturation	5.48E-03	2.00	25
GOBP cell-cell adhesion via plasma- membrane adhesion molecules	4.91E-03	1.81	161	GOBP regulation of neuronal synaptic plasticity	1.77E-03	2.00	53
GOCC glutamatergic synapse	2.58E-04	1.78	296	GOBP regulation of postsynaptic	2.48E-02	1.98	16
GOCC oxidoreductase complex	4.98E-02	1.77	86	neurotransmitter receptor activity			
Postpubertal-enriched versus prepubertal				GOBP cell-cell adhesion via plasma-	9.46E-05	1.94	161
GOBP chromatin organization	3.62E-09	1.99	450	membrane adhesion molecules			
GOMF chromatin DNA binding	7.51E-03	1.98	78	GOBP neuromuscular synaptic	2.94E-02	1.93	15
GOCC intermediate filament	1.96E-02	1.95	42	transmission			
GOBP nucleosome organization	1.57E-02	1.86	68	Adult-enriched versus postpubertal			
GOMF histone binding	1.50E-03	1.82	207	GOCC oxidoreductase complex	6.01E-08	2.44	86
GOBP positive regulation of vasculature	4.40E-02	1.82	76	GOBP aerobic respiration	3.11E-09	2.41	138
development				GOCC mitochondrial protein-	1.44E-11	2.33	242
GOBP histone modification	7.04E-05	1.79	386	containing complex			
GOMF chromatin binding	7.04E-05	1.75	425	GOCC proton-transporting two-sector	3.69E-04	2.29	15
GOBP steroid hormone-mediated	4.40E-02	1.74	102	ATPase complex, catalytic domain			
signaling pathway				GOCC proton-transporting two-sector	5.71E-04	2.18	35
GOMF transcription coregulator activity	1.80E-03	1.64	399	ATPase complex			
				GOBP energy derivation by oxidation of	1.25E-08	2.18	229
				organic compounds			
				GOBP NADH metabolic process	1.30E-03	2.15	28
				GOBP nucleoside triphosphate	3.53E-05	2.14	101
				biosynthetic process			
				GOBP mitochondrial respiratory chain	1.38E-04	2.14	76
				complex assembly			
				GOBP glucose catabolic process	4.11E-03	2.12	18

^a CP=callosal projection; L3PNs=layer 3 pyramidal neurons; NES=normalized enrichment score.

compared to CP L3PNs across age groups, an observation consistent with prior findings that NEFM protein is enriched in IP relative to CP L3PNs (35). In contrast, other genes related to neurite outgrowth were enriched in CP compared to IP L3PNs in all age groups. Among these genes are TIAM1, which controls the cytoskeleton-modulating RAC1 signaling pathway that stimulates axon growth and spine formation (36, 37); ADCYAP1, which activates RAC1 (38); and HGF, which positively controls dendritic length and branching (27).

Gene expression differences between CP and IP L3PNs might also contribute to the electrophysiological diversity among L3PNs in monkey DLPFC (39, 40). For example, genes encoding proteins that regulate excitability, such as the voltage-gated sodium channel subunit genes SCN1A and

SCN1B were enriched in IP neurons, whereas SCN3A was enriched in CP neurons. These enrichment patterns were observed in all age groups, consistent with prior findings that the intrinsic excitability of monkey DLPFC L3PNs achieves a mature state before the prepubertal period (41).

Protracted Maturation of CP and IP L3PN Transcriptomes

The number of DEGs between CP and IP L3PNs nearly doubled between the prepubertal (N=1,046) and post-pubertal (1,942) monkeys and increased by an additional 50% in the adult (3,057) monkeys, consistent with findings in the marmoset neocortex, in which an early postnatal panneuronal transcriptome matures into cell type–specific patterns of gene expression in adulthood (42). These findings

E shows plots of representative genes whose expression levels change in CP and IP L3PNs over different time periods. In each plot, hash bars indicate group means, and filled circles indicate values for individual monkeys; lines connecting the means are included to highlight the different developmental trajectories. CP=callosal projection; DEGs=differentially expressed genes; IP=ipsilateral projection; L3PNs=layer 3 pyramidal neurons; post=postpubertal; pre=prepubertal.

TABLE 3. Selected significant pathways in IP L3PNs differentiating prepubertal and adult animals from postpubertal animals

Pathways	p _{adj}	NES	Size	Pathways	p _{adj}	NES	Size
Prepubertal-enriched versus postpubertal				Postpubertal-enriched versus adult			
GOCC intrinsic component of	2.98E-05	2.34	73	GOCC sarcoplasmic reticulum	1.95E-02	2.06	27
postsynaptic specialization				membrane			
membrane				GOBP learning	4.27E-03		130
GOCC postsynaptic density membrane	1.88E-05		84	GOMF calcium ion transmembrane	1.91E-02	1.87	90
GOBP cell-cell adhesion via plasma-	1.86E-06	2.18	161	transporter activity			
membrane adhesion molecules				GOBP regulation of Rho protein signal	3.60E-02	1.87	62
GOBP neuron cell-cell adhesion	1.11E-02		15	transduction			
GOBP heterophilic cell-cell adhesion	1.11E-02	2.06	28	GOBP regulation of calcium ion	3.40E-02	1.85	63
via plasma membrane cell adhesion				transmembrane transporter activity			
molecules				GOCC site of polarized growth	1.25E-02		156
GOBP regulation of synapse structure or	1.96E-05	2.02	175	GOCC distal axon	2.15E-02		233
activity	0.005.40	4.06	504	GOCC axon	9.73E-04		536
GOBP cell-cell adhesion	2.02E-10		524	GOBP cell morphogenesis involved in	1.95E-02	1.48	550
GOBP morphogenesis of a polarized	1.21E-02	1.86	72	differentiation			
epithelium GOCC filopodium	1.62E-02	1 0 /	81	Adult-enriched versus postpubertal			
GOCC illopodium GOCC glutamatergic synapse	4.30E-05		296	GOCC cytosolic ribosome	3.13E-04		89
3 3 1	4.30E-03	1.60	290	GOMF structural constituent of	3.13E - 04	2.09	148
Postpubertal-enriched versus prepubertal				ribosome			
GOBP positive regulation of sodium ion	2.92E-02	2.02	17	GOBP cytoplasmic translation	8.74E-03		143
transmembrane transport	4065 00	4.05	4.6	GOCC clathrin-coated vesicle	3.47E-02	1.//	148
GOMF aldo-keto reductase NADP activity	4.96E-02	1.95	16				
GOMF kinesin binding	2.63E-02	1.93	39				
GOBP protein homotetramerization	2.44E-02	1.90	40				
GOBP multicellular organismal movement	4.04E-02	1.89	30				
GOCC nucleoid	4.69E-02	1.86	39				
GOCC main axon	2.92E-02	1.86	55				
GOCC T-tubule	4.91E-02	1.82	43				
GOBP striated muscle contraction	1.06E-02	1.82	105				
GOCC mitochondrial matrix	1.88E-05	1.76	403				

^a IP=ipsilateral projection; L3PNs=layer 3 pyramidal neurons; NES=normalized enrichment score.

suggest that even though the axonal projection phenotype of L3PN subtypes is established early in development, their molecular phenotypes—which, as noted above, might contribute to differences in other anatomical or functional properties—continue to mature into adulthood.

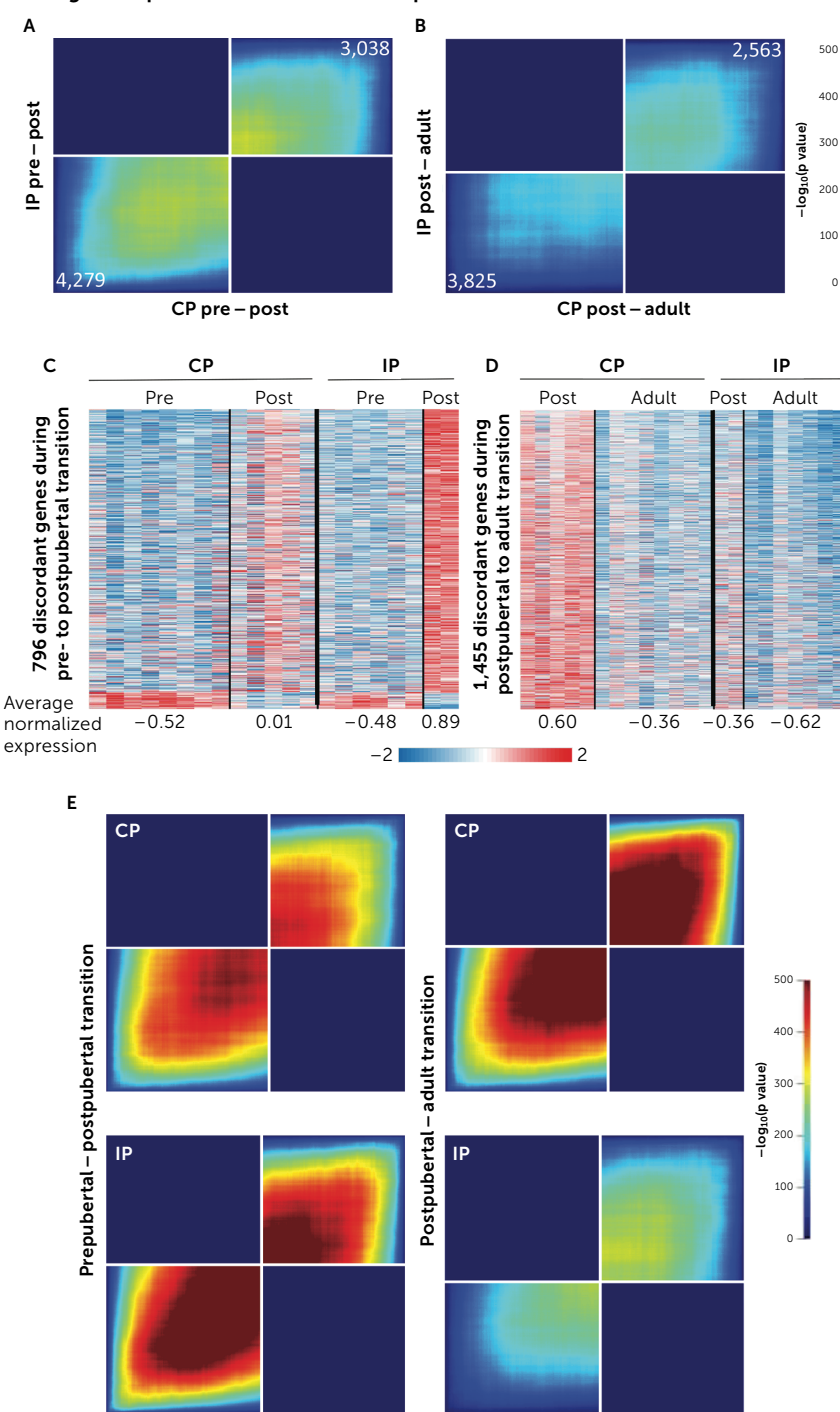
Together, these findings demonstrate that even in the same brain region and cortical layer, L3PN subtypes that differ in their axonal projection targets show a progressive emergence of distinct transcriptomes that continues across late postnatal development into adulthood. These protracted shifts in gene expression across late postnatal development in both CP and IP L3PNs likely contribute to the protracted refinement of layer 3 DLPFC circuitry (1, 43) and thus to the maturation of DLPFC-mediated cognitive abilities that are mediated by this circuitry (44, 45).

The temporal expression patterns of specific genes may provide insight into the molecular basis for the maturation of aspects of layer 3 DLPFC circuitry. For example, the similar increases (\sim 40%) in NEFM expression between prepubertal and adult monkeys in both CP and IP L3PNs might support the stabilization of mature axons (34). In contrast, the similar declines (\sim 50%) in expression of SEMA5B, which regulates the formation of synaptic connections (46), between prepuberty and adulthood in both PN subtypes might contribute

to the decrease in density of axospinous synapses in DLPFC layer 3 across adolescence (13).

The activity of PNs is regulated by inhibition mediated by GABAA receptors composed of different subunits. Consistent with a prior developmental study of random samples of monkey DLPFC L3PNs (47), we found that GABRG2 subunit mRNA levels increased with age in both L3PN subtypes but were lower in IP than CP neurons at all ages. Given that the GABRG2 is present in most synaptic GABAA receptors (GABAARs) (48) and is required for postsynaptic receptor clustering (49), these findings suggest that the control of PN activity by synaptic inhibition increases with age in both L3PN subtypes but is consistently greater in CP than IP neurons across late postnatal development and into adulthood. In contrast, GABRA2 mRNA levels decreased with age only in CP L3PNs but were still lower in IP than CP L3PNs at all three ages. Given that the presence of the GABRA2 subunit is associated with slower decay times of GABAAR-activated currents (50), our findings suggest that IP and CP L3PNs progressively differ with age in the decay kinetics of the synaptic response to GABA, which might differentially affect their engagement in oscillatory activity. For example, CP L3PNs might be more likely to participate in networks with slower beta frequency oscillations and IP

FIGURE 5. RRHO2 analyses of gene expression shifts over development^a



Prepubertal - adult transition

^a Panels A and B are rank-rank hypergeometric overlap (RRHO) plots, from analyses performed using the R package RRHO2, of gene expression differences between prepubertal and postpubertal monkeys for CP and IP L3PNs (panel A) and between postpubertal and adult monkeys for CP and IP L3PNs (panel B). The numbers of concordant genes that increase (lower left quadrant) or decrease (upper right quadrant) in expression level with age are shown. Panels C and D are heat maps of the discordant genes from the prepubertal-to-postpubertal transition (panel C) and from the postpubertal-to-adult transition (panel D). Each column of the heat maps represents an individual animal for the indicated cell type and each row an individual gene. The numbers below each heat map are the average normalized expression level for all the discordant genes in that cell type and age group. Note that for the prepubertal-to-postpubertal transition, the shift in gene expression is larger for IP than for CP L3PNs, whereas for the postpubertal-to-adult transition, the shift in gene expression is larger for CP than for IP L3PNs. The RRHO2 plots in panel E show gene expression differences between the prepubertal and adult age groups compared to the prepubertal-to-postpubertal transition (left side) and the postpubertal-to-adult transition (right side) for CP L3PNs (top) and IP L3PNs (bottom). The earlier transition accounts for most of the overall difference with age for IP L3PNs, whereas the later transition accounts for more of the overall difference with age for CP L3PNs approached projection; L3PNs=layer 3 pyramidal neurons; post=postpubertal; pre=prepubertal.

L3PNs in networks with faster gamma frequency oscillations (41). Given that beta and gamma frequency oscillations play different roles in working memory (51), our findings support the idea that IP and CP L3PNs differentially contribute to subcomponents of working memory processing (5–8).

IP Neurons Express a Mature Transcriptome Earlier Than CP Neurons

The timing of large (≥15%) shifts in gene expression differed between IP and CP neurons, with most of these large shifts in IP L3PNs occurring between prepubertal and postpubertal monkeys, whereas in CP L3PNs most large shifts occurred between the postpubertal and adult age groups. Consistent with these findings, the RRHO2 analyses demonstrated that for a subset of genes, the shift in gene expression between prepubertal and postpubertal monkeys was greater in IP L3PNs, whereas the shift in gene expression between postpubertal and adult monkeys was greater in CP L3PNs.

Together, these differences suggest that IP L3PNs approach a mature transcriptome earlier in development than CP L3PNs. These cell type differences might reflect differences in the timing of the maturation of the cortical areas targeted by their axons given that axonal projection target appears to be an important determinant of a neuron's transcriptome (16, 52, 53). Consistent with this interpretation, neuroimaging studies (54, 55) indicate that the PPC (the target region of our IP L3PNs) matures earlier than the DLPFC (the target region of our CP L3PNs).

Implications for Schizophrenia

Our findings have several potential implications for understanding some of the core deficits in schizophrenia. The distinct transcriptome profiles of CP and IP neurons in the adult monkey suggest that these two subtypes of L3PNs might be identifiable in single nucleus RNA sequencing studies of the postmortem human brain. Such findings could then be used to address the long-standing question of whether the well-established morphological (e.g., fewer dendritic spines [56, 57]) and molecular (e.g., lower expression of mitochondrial genes [58]) alterations of L3PNs in schizophrenia are common to all PNs in this laminar location or are cell type specific. For example, the enrichment of mitochondria-associated pathways in IP L3PNs compared to CP L3PNs suggests that these two neuronal subtypes might differ in their susceptibility to the expression deficits of genes related to oxidative phosphorylation previously reported in DLPFC L3PNs in schizophrenia (58). Answering this question will reveal the generality or specificity of DLPFC circuitry alterations in schizophrenia and thus inform the selection of targets for therapeutic interventions.

Our findings also suggest new perspectives on the pathogenesis of L3PN alterations in schizophrenia. The later transcriptional maturation of CP L3PNs is associated with a decrease in multiple pathways involved in synaptic function between the postpubertal and adult ages. Given that dendritic spine density declines on L3PNs in monkey DLPFC

during this developmental period (59), these findings suggest that CP L3PNs might be preferentially vulnerable to the proposed disease process of excessive synaptic pruning in schizophrenia (15, 60). In addition, the presence of transcriptome shifts in both cell types during the peripubertal period suggests that alterations to either or both of these developmental processes could contribute to the emergence of cognitive impairments during early adolescence in individuals who are later diagnosed with schizophrenia (17–21).

AUTHOR AND ARTICLE INFORMATION

Department of Psychiatry (Arion, Enwright, Gonzalez-Burgos, Lewis) and Department of Neuroscience (Lewis), University of Pittsburgh, Pittsburgh.

Send correspondence to Dr. Lewis (lewisda@upmc.edu).

Supported by NIMH grant MH051234 to Dr. Lewis.

The authors thank Kate Gurnsey and Sam Dienel for assistance with surgical procedures and Kelly Rogers and Mary Brady for technical assistance.

Dr. Lewis receives investigator-initiated research support from Merck. The other authors report no financial relationships with commercial interests.

Received July 6, 2023; revisions received December 4, 2023, and February 29, 2024; accepted April 4, 2024.

REFERENCES

- Dienel SJ, Schoonover KE, Lewis DA: Cognitive dysfunction and prefrontal cortical circuit alterations in schizophrenia: developmental trajectories. Biol Psychiatry 2022; 92:450–459
- Andersen RA, Asanuma C, Cowan WM: Callosal and prefrontal associational projecting cell populations in area 7A of the macaque monkey: a study using retrogradely transported fluorescent dyes. J Comp Neurol 1985; 232:443–455
- Schwartz ML, Goldman-Rakic PS: Single cortical neurones have axon collaterals to ipsilateral and contralateral cortex in fetal and adult primates. Nature 1982; 299:154–155
- Schwartz ML, Goldman-Rakic PS: Callosal and intrahemispheric connectivity of the prefrontal association cortex in rhesus monkey: relation between intraparietal and principal sulcal cortex. J Comp Neurol 1984: 226:403–420
- Brincat SL, Donoghue JA, Mahnke MK, et al: Interhemispheric transfer of working memories. Neuron 2021; 109:1055–1066.e4
- Hart E, Huk AC: Recurrent circuit dynamics underlie persistent activity in the macaque frontoparietal network. Elife 2020; 9: e52460
- 7. Goldman-Rakic PS: Cellular basis of working memory. Neuron 1995; 14:477–485
- Constantinidis C, Wang XJ: A neural circuit basis for spatial working memory. Neuroscientist 2004; 10:553–565
- 9. Luna B, Padmanabhan A, O'Hearn K: What has fMRI told us about the development of cognitive control through adolescence? Brain Cogn 2010; 72:101–113
- Kolk SM, Rakic P: Development of prefrontal cortex. Neuropsychopharmacology 2022; 47:41–57
- Meissirel C, Dehay C, Berland M, et al: Segregation of callosal and association pathways during development in the visual cortex of the primate. J Neurosci 1991; 11:3297–3316
- Schwartz ML, Goldman-Rakic PS: Prenatal specification of callosal connections in rhesus monkey. J Comp Neurol 1991; 307: 144–162
- 13. Bourgeois JP, Goldman-Rakic PS, Rakic P: Synaptogenesis in the prefrontal cortex of rhesus monkeys. Cereb Cortex 1994; 4:78–96

- Anderson SA, Classey JD, Condé F, et al: Synchronous development of pyramidal neuron dendritic spines and parvalbumin-immunoreactive chandelier neuron axon terminals in layer III of monkey prefrontal cortex. Neuroscience 1995; 67:7–22
- Petanjek Z, Judaš M, Šimic G, et al: Extraordinary neoteny of synaptic spines in the human prefrontal cortex. Proc Natl Acad Sci U S A 2011; 108:13281–13286
- Arion D, Enwright JF, Gonzalez-Burgos G, et al: Differential gene expression between callosal and ipsilateral projection neurons in the monkey dorsolateral prefrontal and posterior parietal cortices. Cereb Cortex 2023; 33:1581–1594
- Meier MH, Caspi A, Reichenberg A, et al: Neuropsychological decline in schizophrenia from the premorbid to the postonset period: evidence from a population-representative longitudinal study. Am J Psychiatry 2014; 171:91–101
- Gur RC, Calkins ME, Satterthwaite TD, et al: Neurocognitive growth charting in psychosis spectrum youths. JAMA Psychiatry 2014: 71:366–374
- MacCabe JH, Wicks S, Löfving S, et al: Decline in cognitive performance between ages 13 and 18 years and the risk for psychosis in adulthood: a Swedish longitudinal cohort study in males. JAMA Psychiatry 2013; 70:261–270
- Reichenberg A, Caspi A, Harrington H, et al: Static and dynamic cognitive deficits in childhood preceding adult schizophrenia: a 30-year study. Am J Psychiatry 2010; 167:160–169
- Mollon J, David AS, Zammit S, et al: Course of cognitive development from infancy to early adulthood in the psychosis spectrum. JAMA Psychiatry 2018; 75:270–279
- 22. Ritchie ME, Phipson B, Wu D, et al: *limma* powers differential expression analyses for RNA-sequencing and microarray studies. Nucleic Acids Res 2015; 43:e47
- Johnson WE, Li C, Rabinovic A: Adjusting batch effects in microarray expression data using empirical Bayes methods. Biostatistics 2007; 8:118–127
- 24. Korotkevich G, Sukhov V, Sergushichev A: Fast gene set enrichment analysis. bioRxiv, October 22, 2019
- Cahill KM, Huo Z, Tseng GC, et al: Improved identification of concordant and discordant gene expression signatures using an updated rank-rank hypergeometric overlap approach. Sci Rep 2018; 8:9588
- Arion D, Unger T, Lewis DA, et al: Molecular markers distinguishing supragranular and infragranular layers in the human prefrontal cortex. Eur J Neurosci 2007; 25:1843–1854
- Finsterwald C, Martin JL: Cellular mechanisms underlying the regulation of dendritic development by hepatocyte growth factor. Eur J Neurosci 2011; 34:1053–1061
- Schafer ST, Han J, Pena M, et al: The Wnt adaptor protein ATP6AP2 regulates multiple stages of adult hippocampal neurogenesis. J Neurosci 2015; 35:4983–4998
- Emery AC, Eiden MV, Mustafa T, et al: Rapgef2 connects GPCRmediated cAMP signals to ERK activation in neuronal and endocrine cells. Sci Signal 2013; 6:ra51
- Duman JG, Tzeng CP, Tu YK, et al: The adhesion-GPCR BAI1 regulates synaptogenesis by controlling the recruitment of the Par3/Tiam1 polarity complex to synaptic sites. J Neurosci 2013; 33:6964–6978
- 31. Arlotta P, Molyneaux BJ, Chen J, et al: Neuronal subtype-specific genes that control corticospinal motor neuron development in vivo. Neuron 2005; 45:207–221
- Nowakowski TJ, Bhaduri A, Pollen AA, et al: Spatiotemporal gene expression trajectories reveal developmental hierarchies of the human cortex. Science 2017; 358:1318–1323
- Soloway AS, Pucak ML, Melchitzky DS, et al: Dendritic morphology of callosal and ipsilateral projection neurons in monkey prefrontal cortex. Neuroscience 2002; 109:461–471
- Innocenti GM, Price DJ: Exuberance in the development of cortical networks. Nat Rev Neurosci 2005; 6:955–965

- 35. Hof PR, Nimchinsky EA, Morrison JH: Neurochemical phenotype of corticocortical connections in the macaque monkey: quantitative analysis of a subset of neurofilament protein-immunoreactive projection neurons in frontal, parietal, temporal, and cingulate cortices. J Comp Neurol 1995; 362:109–133
- 36. Ehler E, Van Leeuwen F, Collard JG, et al: Expression of Tiam-1 in the developing brain suggests a role for the Tiam-1-Rac signaling pathway in cell migration and neurite outgrowth. Mol Cell Neurosci 1997; 9:1–12
- Tolias KF, Bikoff JB, Burette A, et al: The Rac1-GEF Tiam1 couples the NMDA receptor to the activity-dependent development of dendritic arbors and spines. Neuron 2005; 45: 525-538
- 38. Sakai Y, Hashimoto H, Shintani N, et al: PACAP activates Rac1 and synergizes with NGF to activate ERK1/2, thereby inducing neurite outgrowth in PC12 cells. Brain Res Mol Brain Res 2004: 123:18-26
- Zaitsev AV, Povysheva NV, Gonzalez-Burgos G, et al: Electrophysiological classes of layer 2/3 pyramidal cells in monkey prefrontal cortex. J Neurophysiol 2012; 108:595–609
- González-Burgos G, Miyamae T, Krimer Y, et al: Distinct properties of layer 3 pyramidal neurons from prefrontal and parietal areas of the monkey neocortex. J Neurosci 2019; 39:7277–7290
- 41. Gonzalez-Burgos G, Cho RY, Lewis DA: Alterations in cortical network oscillations and parvalbumin neurons in schizophrenia. Biol Psychiatry 2015; 77:1031–1040
- 42. Yuan W, Ma S, Brown JR, et al: Temporally divergent regulatory mechanisms govern neuronal diversification and maturation in the mouse and marmoset neocortex. Nat Neurosci 2022; 25: 1049–1058
- Hoftman GD, Lewis DA: Postnatal developmental trajectories of neural circuits in the primate prefrontal cortex: identifying sensitive periods for vulnerability to schizophrenia. Schizophr Bull 2011; 37:493–503
- 44. Uhlhaas PJ, Roux F, Singer W, et al: The development of neural synchrony reflects late maturation and restructuring of functional networks in humans. Proc Natl Acad Sci U S A 2009; 106: 9866–9871
- Constantinidis C, Luna B: Neural substrates of inhibitory control maturation in adolescence. Trends Neurosci 2019; 42: 604-616
- O'Connor TP, Cockburn K, Wang W, et al: Semaphorin 5B mediates synapse elimination in hippocampal neurons. Neural Dev 2009; 4:18
- 47. Datta D, Arion D, Lewis DA: Developmental expression patterns of GABAA receptor subunits in layer 3 and 5 pyramidal cells of monkey prefrontal cortex. Cereb Cortex 2015; 25:2295–2305
- 48. Angelotti TP, Macdonald RL: Assembly of GABAA receptor subunits: alpha 1 beta 1 and alpha 1 beta 1 gamma 2S subunits produce unique ion channels with dissimilar single-channel properties. J Neurosci 1993; 13:1429–1440
- Alldred MJ, Mulder-Rosi J, Lingenfelter SE, et al: Distinct gamma2 subunit domains mediate clustering and synaptic function of postsynaptic GABAA receptors and gephyrin. J Neurosci 2005; 25:594–603
- Lavoie AM, Tingey JJ, Harrison NL, et al: Activation and deactivation rates of recombinant GABA(A) receptor channels are dependent on alpha-subunit isoform. Biophys J 1997; 73:2518–2526
- Lundqvist M, Brincat SL, Rose J, et al: Working memory control dynamics follow principles of spatial computing. Nat Commun 2023; 14:1429
- 52. Klingler E, De la Rossa A, Fièvre S, et al: A translaminar genetic logic for the circuit identity of intracortically projecting neurons. Curr Biol 2019; 29:332–339.e5
- Sorensen SA, Bernard A, Menon V, et al: Correlated gene expression and target specificity demonstrate excitatory projection neuron diversity. Cereb Cortex 2015; 25:433–449

- 54. Gogtay N, Giedd JN, Lusk L, et al: Dynamic mapping of human cortical development during childhood through early adulthood. Proc Natl Acad Sci U S A 2004; 101:8174–8179
- 55. Gerván P, Soltész P, Filep O, et al: Posterior-anterior brain maturation reflected in perceptual, motor and cognitive performance. Front Psychol 2017; 8:674
- Garey LJ, Ong WY, Patel TS, et al: Reduced dendritic spine density on cerebral cortical pyramidal neurons in schizophrenia. J Neurol Neurosurg Psychiatry 1998; 65:446–453
- Glantz LA, Lewis DA: Decreased dendritic spine density on prefrontal cortical pyramidal neurons in schizophrenia. Arch Gen Psychiatry 2000; 57:65–73

934

- 58. Arion D, Corradi JP, Tang S, et al: Distinctive transcriptome alterations of prefrontal pyramidal neurons in schizophrenia and schizoaffective disorder. Mol Psychiatry 2015; 20: 1307–1405
- 59. Gonzalez-Burgos G, Miyamae T, Nishihata Y, et al: Strength of excitatory inputs to layer 3 pyramidal neurons during synaptic pruning in the monkey prefrontal cortex: relevance for the pathogenesis of schizophrenia. Biol Psychiatry 2023; 94: 288–296
- Feinberg I: Schizophrenia: caused by a fault in programmed synaptic elimination during adolescence? J Psychiatr Res 1982; 17: 319–334